

Chemical Science

Accepted Manuscript

This article can be cited before page numbers have been issued, to do this please use: X. Wang, N. Yan, M. Xie, P. Liu, P. Bai, H. Su, B. Wang, Y. Wang, L. Li, T. Cheng, P. Guo, W. Yan and J. Yu, *Chem. Sci.*, 2021, DOI: 10.1039/D1SC00619C.



This is an Accepted Manuscript, which has been through the Royal Society of Chemistry peer review process and has been accepted for publication.

Accepted Manuscripts are published online shortly after acceptance, before technical editing, formatting and proof reading. Using this free service, authors can make their results available to the community, in citable form, before we publish the edited article. We will replace this Accepted Manuscript with the edited and formatted Advance Article as soon as it is available.

You can find more information about Accepted Manuscripts in the [Information for Authors](#).

Please note that technical editing may introduce minor changes to the text and/or graphics, which may alter content. The journal's standard [Terms & Conditions](#) and the [Ethical guidelines](#) still apply. In no event shall the Royal Society of Chemistry be held responsible for any errors or omissions in this Accepted Manuscript or any consequences arising from the use of any information it contains.

ARTICLE

Inorganic cation-tailored “trapdoor” effect of the silicoaluminophosphate zeolite for highly selective CO₂ separationXiaohe Wang,^[a] Nana Yan,^[b] Miao Xie,^[c] Puxu Liu,^[d] Pu Bai,^[a] Haopeng Su,^[a] Binyu Wang,^[a] Yunzheng Wang,^[a] Libo Li,^[d] Tao Cheng,^[c] Peng Guo^{*[b]}, Wenfu Yan,^{*[a]} Jihong Yu^{*[a,e]}Received 00th January 20xx,
Accepted 00th January 20xx

DOI: 10.1039/x0xx00000x

Functional nanoporous materials are widely explored for CO₂ separation, in particular small-pore aluminosilicate zeolites having “trapdoor” effect. Such effect allows the specific adsorbate to push away the sited cations inside the window followed by exclusive admission to the zeolite pores, which is more advantageous for highly selective CO₂ separation. Herein, we demonstrated that the protonated organic structure-directing agent in the small-pore silicoaluminophosphate (SAPO) **RHO** zeolite can be directly exchanged with Na⁺, K⁺, or Cs⁺ and that the Na⁺ form of SAPO-RHO exhibited an unprecedented separation for CO₂/CH₄, superior to all of the nanoporous materials reported to date. Rietveld refinement revealed that Na⁺ sited the center of the single eight-membered ring (s8r), while the K⁺ and Cs⁺ sited the center of the double 8-rings (d8rs). Theoretical calculations showed that the interaction between the Na⁺ and the s8r in SAPO-RHO was stronger than that in aluminosilicate **RHO**, giving an enhanced “trapdoor” effect and record high selectivity for CO₂ with the separation factor of 2196 for CO₂/CH₄ (0.02/0.98 bar). The separation factor of Na-SAPO-RHO for CO₂/N₂ was 196, which was the top level among zeolitic materials. This work opens a new avenue for gas separation by using diverse silicoaluminophosphate zeolites in terms of cation-tailored “trapdoor” effect.

Introduction

The CO₂ concentration in the atmosphere has increased rapidly in recent decades due to the dramatic increase of emissions from industries and power plants, which is believed to have significant influence on global warming.^[1] In CO₂ capture and sequestration (CCS), two important issues are the separation of CO₂ from post-combustion (CO₂/N₂) and natural gas mixtures (CO₂/CH₄).^[2] Industrially, the separation of CO₂/CH₄ and CO₂/N₂ is mainly based on the strong chemical adsorption of amine solution to CO₂, which has the drawbacks of complicated operation, strong corrosiveness to equipment, high energy consumption for regeneration, and easy deactivation. Hence, the low-cost and high-efficiency capture and separation of CO₂ have always been highly desired.^[2a, 3]

Compared to the chemical adsorption, the weak physical adsorption based processes for the separation of CO₂/CH₄ and

CO₂/N₂ have attracted much attention due to the characteristics of clean, simple operation, and low-energy consumption.^[4] Over recent years, a variety of solid porous materials have been investigated for the separation of CO₂/CH₄ and CO₂/N₂,^[2a, 2c, 3b, 5] including carbon-based materials,^[6] zeolites,^[7] metal-organic frameworks (MOFs),^[8] N or amine-functionalized solid porous materials,^[9] porous organic solids, etc.^[10] Taking into account the key factors governing the separation efficiency of CO₂ such as adsorption capacity, selectivity, adsorption/desorption kinetics, and cost, zeolites, in particular the small-pore zeolites with “trapdoor” effect, have more advantages over other materials for industrial utilizations.^[4a, 4b]

“Trapdoor” effect of zeolites was first observed in the small-pore chabazite (**CHA**) zeolites that can even perform “size-inverse” separation.^[11] For the chabazite structure with a low Si/Al ratio (<3), K⁺, Rb⁺, or Cs⁺ ions fully occupy 8-ring windows that connect the *cha* cages. Larger molecule of CO has a stronger interaction with the cations than smaller molecule of N₂ does, which induces temporary and reversible cation deviation from the window sites and allows for exclusive admission of CO (0.376 nm) instead of N₂ (0.364 nm). Such separation also gives a high selectivity of 93 for CO₂/CH₄ separation over a large pressure range.^[11]

^a State Key Laboratory of Inorganic Synthesis and Preparative Chemistry, College of Chemistry, Jilin University, Changchun 130012, China. E-mail: yanw@jlu.edu.cn; jihong@jlu.edu.cn

^b National Engineering Laboratory for Methanol to Olefins, Dalian National Laboratory for Clean Energy, Dalian Institute of Chemical Physics, Chinese Academy of Sciences, Dalian 116023, China. E-mail: pguo@dicp.ac.cn

^c Institute of Functional Nano & Soft Materials (FUNSOM) and Jiangsu Key Laboratory for Carbon-Based Functional Materials & Devices, Soochow University, Suzhou 215123, China

^d College of Chemistry and Chemical Engineering, Shanxi Key Laboratory of Gas Energy Efficient and Clean Utilization, Taiyuan University of Technology, Taiyuan 030024, Shanxi, China

^e International Center of Future Science, Jilin University, Changchun 130012, China
Electronic Supplementary Information (ESI) available: Details for synthesis, ion-exchange, characterizations, and simulation. CCDC 2056929, 2056930, 2056931, and 2056932. See DOI: 10.1039/x0xx00000x



Among the small-pore zeolites, aluminosilicate Rho (**RHO**) with remarkable structural flexibility was found to have high selectivity for CO₂ in the separation of CO₂ and CH₄.^[12] The idealized **RHO** framework (space group: $Im\bar{3}m$) is constructed by double 8-rings (*d8rs*) and *lta* cages as the composite building units (CBUs). Each *lta* cage connects with six *d8rs* in six directions in space, while each *d8r* links two *lta* cages, generating a three-dimensional (3D) channel system with 8-ring pore openings (0.36 nm × 0.36 nm).^[13]

Previous studies show that the hydrated cation form and the dehydrated proton form of zeolite Rho have the highest symmetry of $Im\bar{3}m$. The framework of dehydrated cation form of zeolite Rho undergoes distortions to the non-centrosymmetric $I43m$.^[14] During the distortion, the 8-ring geometry is twisted from a circle to an elliptical shape, which reduces the pore aperture and thus adjusts the separation selectivity. Alteration in the type of cations can not only distort the 8-ring geometry but also tune the interaction between the cations and the adsorbates. Notably, the “trapdoor” effect in the dehydrated cation form of zeolite Rho was observed in the selective separation of CO₂/CH₄.^[14c, 15] Zeolite Rho showed an exceptional high selectivity for CO₂ in the separation of CO₂/CH₄ and the separation factor was as high as 960, which becomes a benchmark set by zeolites in the separation of CO₂ from CH₄.^[14c, 15a]

SAPO **RHO**-type, denoted as DNL-6 (hereafter denoted as SAPO-RHO), was firstly synthesized by Su *et al.* with diethylamine (DEA) as organic structure-directing agent (OSDA) in the presence of cetyltrimethylammonium bromide (CTAB) in 2011.^[16] Recently, a series of commercialized OSDAs were identified with a novel approach called **RSS** (Refining, Summarizing, and Searching) for the successful synthesis of SAPO-RHO.^[17] Considering the remarkable CO₂ selectivity of the cationic forms of aluminosilicate **RHO** attributed to its “trapdoor” effect, we suppose that the cationic forms of SAPO-RHO might have a better CO₂ selectivity because the framework of silicoaluminophosphate is more flexible than that of aluminosilicate and the “trapdoor” effect in SAPO could be well tailored. However, in general, the introduction of inorganic cations to the SAPO-RHO via conventional ion-exchange of cations with the protonated SAPO-RHO zeolite will inevitably result in a serious crystallinity loss or even collapse of the framework.^[7c, 18]

Herein, we prepared the inorganic cationic forms of SAPO-RHO zeolites via a direct ion-exchange of OSDA⁺-containing SAPO-RHO with Na⁺, K⁺, or Cs⁺. The Na⁺ form of SAPO-RHO (denoted as Na-SAPO-RHO) with optimized cation content showed unprecedented selective separation performance for CO₂ from CH₄ and N₂. Rietveld refinement and theoretical calculations provided an insight into the intriguing CO₂ separation performance arising from the pronounced “trapdoor” effect. Breakthrough experiments suggested that Na-SAPO-RHO is a promising candidate for CO₂ capture in natural gas purification and flue gas separation via adsorption-based separation processes.

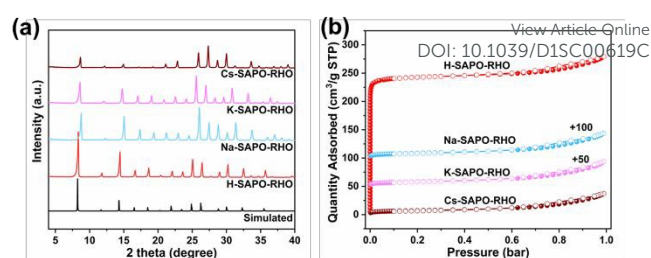


Fig. 1 (a) Simulated XRD pattern of SAPO-RHO and experimental ones of the calcined M-SAPO-RHOs; (b) N₂ adsorption/desorption isotherms of the calcined SAPO-RHO (H-SAPO-RHO) and M-SAPO-RHOs (M=Na, K, and Cs) at 77 K.

Results and discussion

The SAPO-RHO with the Si/(Si+Al+P) mole ratio of 0.18 was hydrothermally synthesized in the presence of DEA, CTAB, and seed at 473 K for 48 h. The direct ion-exchange (three cycles) of the Na⁺, K⁺, or Cs⁺ salt solution with the as-synthesized SAPO-RHO was performed and the resultant product is denoted as M-SAPO-RHO (M = Na, K, and Cs). The exchange degree for Na⁺, K⁺, and Cs⁺ is 87.13, 65.75, and 72.87%, respectively. The detailed information of the synthesis and ion exchange is provided in the Supporting Information. The powder X-ray diffraction (PXRD) (Fig. S1) and the scanning electron microscopy (SEM) analyses (Fig. S2) on the as-synthesized SAPO-RHO and the ion-exchanged M-SAPO-RHOs show that all the SAPO-RHOs are well-defined crystals with high crystallinity. Fig. 1a shows the PXRD patterns of the H-SAPO-RHO and the calcined M-SAPO-RHOs (873 K in air for 4 h). It is worth noting that the diffraction peaks of the calcined M-SAPO-RHO samples obviously shift to high angle compared with those of the H-SAPO-RHO and the simulated XRD of idealized **RHO** framework, indicating the constriction of the unit cell and the distortion of the framework. The texture properties of the SAPO-RHOs were characterized by the N₂ adsorption/desorption at 77 K (Table S1) and the corresponding isotherms are provided in Fig. 1b. Compared with H-SAPO-RHO, the N₂ adsorption of M-SAPO-RHOs was greatly restricted, as observed in zeolite Rho.^[15a]

The unit cell compositions of the calcined SAPO-RHOs as given in Table S1 were determined based on Energy-dispersive spectroscopy (EDS). The EDS mapping (Fig. S3) analysis clearly shows that the Na⁺, K⁺, or Cs⁺ ions are uniformly distributed in the framework of corresponding SAPO-RHO.

Considering the fact of that the separation investigations were performed under the dry condition, we analyzed the structures of dehydrated M-SAPO-RHOs via Rietveld refinement against PXRD data. Here we take Na-SAPO-RHO as example to illustrate the Rietveld refinement process. The initial SAPO-RHO structural model was deduced from the idealized **RHO** framework. Since the alternating distribution of Al and P in the SAPO-RHO framework, its space group was reduced to $I432$ (No. 211) from $Im\bar{3}m$ (No. 229). However, it was very challenging to achieve reasonable refinement results for dehydrated Na-SAPO-RHO (denoted as de-Na-SAPO-RHO) based on the $I432$ space group, since its bond lengths and bond angles deviate heavily from the idealized one. After scrutinizing the cubic unit cell parameter of de-Na-SAPO-RHO ($a = 14.47$ Å), it is quite close



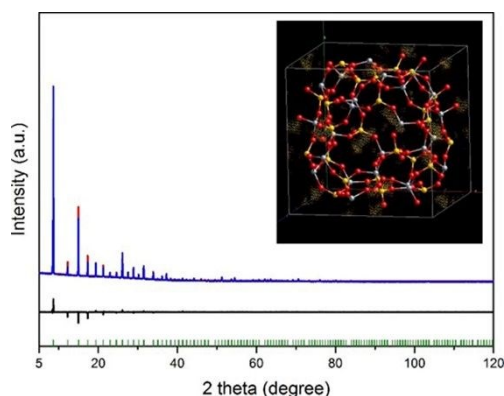


Fig. 2 Plots for locating the Na⁺ ions in the de-Na-SAPO-RHO by applying the appropriate scale factor to the whole pattern. The inset is the difference electron density map to locate initial positions of Na⁺ through Rietveld refinement. The observed, calculated, and difference curves are in blue, red, and black, respectively. The vertical bars indicate the positions of the Bragg peaks ($\lambda=1.5406\text{\AA}$).

to the one of dehydrated distorted zeolite Na-Rho ($a = 14.38\text{\AA}$),^[15a] indicating the crystallographic structure of de-Na-SAPO-RHO becomes distorted from the ideal framework as well. A distorted SAPO-RHO structural model (space group $I23$) was constructed based on the dehydrated distorted zeolite Na-Rho ($I\bar{4}3m$), including the initial atomic coordinates for Al, P, and four O atoms in the asymmetric unit. Table S2 shows the space group changes of the H-type and dehydrated cation exchanged zeolite Rho and SAPO-RHO.

After profile fitting and optimizing the framework, the scale factor between the simulated PXRD data of the optimized framework and the experimental PXRD data was identified against high angle PXRD data ($2\theta: 60^\circ\text{--}120^\circ$), where the influence of the extra-framework species (Na⁺) in the cavities was negligible. Subsequently, the electron difference density map was calculated by applying the scale factor to the entire range (Fig. 2). Since the guest water molecules were already excluded, the isolated electron density within the cavity indicated the initial positions of the Na⁺ ions (inset of Fig. 2). Final Rietveld refinement converged at $R_p=0.0147$, $R_{wp}=0.0213$, and $GOF=1.526$, which revealed that most of Na⁺ ions located in the elliptical single 8-rings (*s8rs*) and coordinated with framework O atoms (closest Na-O distance: 2.540\AA) and the other fraction (1.92 Na^+ ions per unit cell in average) located close to the single 6-rings (*s6rs*) of *lta* cage as shown in Fig. 3a.

Locations and occupancies of K⁺ and Cs⁺ ions in the de-K-SAPO-RHO and de-Cs-SAPO-RHO were determined by utilizing the same method. Unlike Na⁺ ions sitting the center of *s8rs*, the K⁺ ions in the de-K-SAPO-RHO locates at the *d8rs* (center) with the closest K-O distance of 2.713\AA (Fig. 3b). In addition, a small portion of K⁺ ions (0.88 per unit cell) settle at the side of *s6rs* of the *lta* cage. For de-Cs-SAPO-RHO, Cs⁺ ions reside in the center of *d8rs* (closest Cs-O distance: 3.185\AA), while a few of Cs⁺ ions (0.6 per unit cell) are close to the center of *s6r* (Fig. 3c). It is worth noting that cations transfer from *s8r* to *d8r* with the

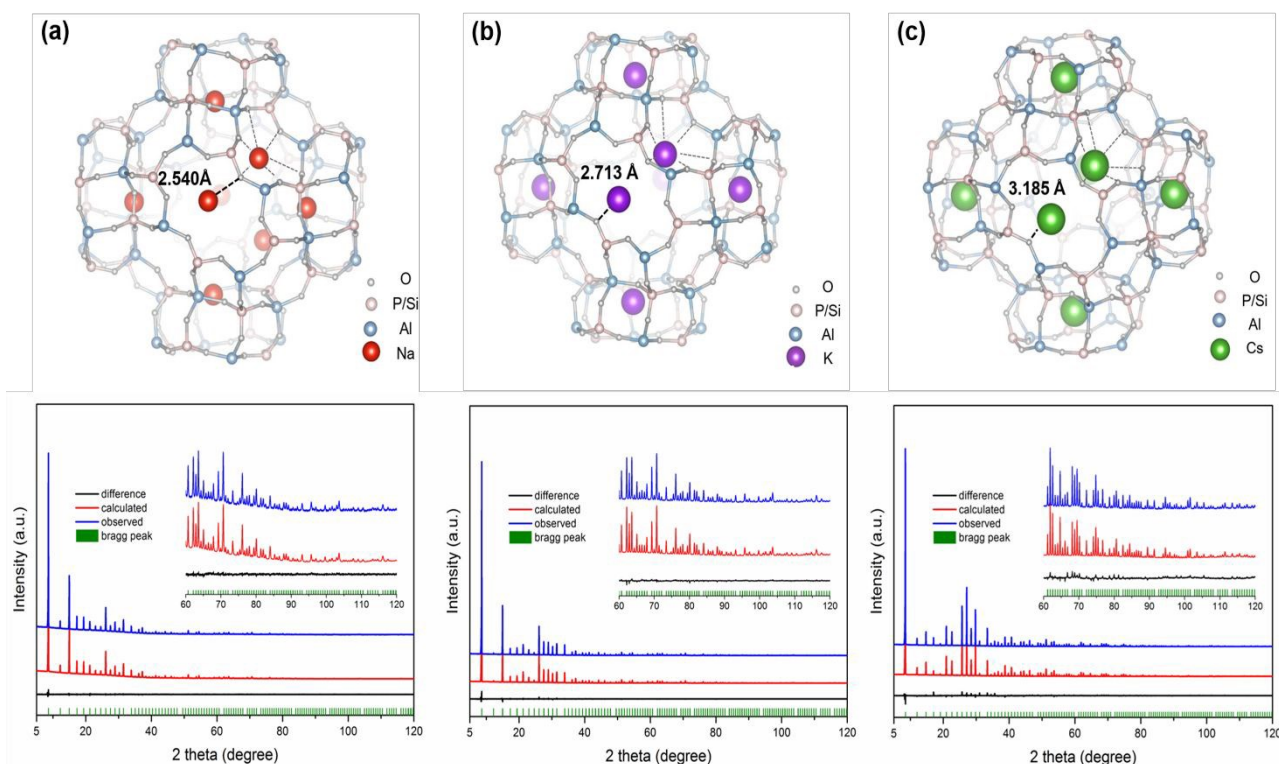


Fig. 3 Crystallographic structures of (a) de-Na-SAPO-RHO, (b) de-K-SAPO-RHO, and (c) de-Cs-SAPO-RHO and their corresponding final Rietveld refinement plots. The observed, calculated, and difference curves are in blue, red, and black, respectively. The vertical bars indicate the positions of the Bragg peaks ($\lambda=1.5406\text{\AA}$).



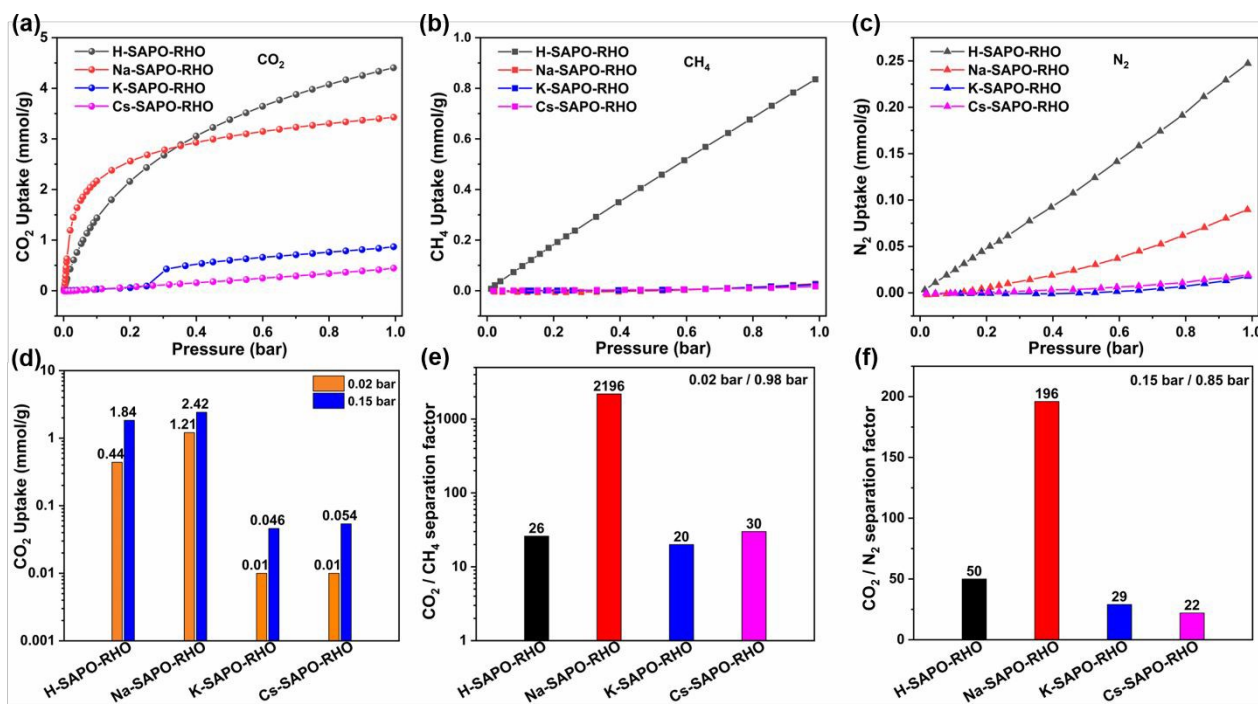


Fig. 4 Comparison of the (a) CO_2 , (b) CH_4 , and (c) N_2 adsorption isotherms of all SAPO-RHOs at 298 K between 0–1 bar; (d) Comparison of the CO_2 uptake for all SAPO-RHOs under 0.02 and 0.15 bar at 298 K respectively; (e) CO_2/CH_4 separation factors at 0.02/0.98 bar and (f) CO_2/N_2 separation factors at 0.15/0.85 bar at 298 K for all SAPO-RHOs.

increase of the atomic number of the alkaline metal ($\text{Na} < \text{K} < \text{Cs}$), resulting from a gradually prolonged cation–O bond distance. The detailed structural data for all SAPO-RHOs are given in Table S3 and Table S4.

To further investigate the structural distortion in cation exchanged SAPO-RHO, a control sample of hydrated Cs-SAPO-RHO was measured. It is worth noting that the unit cell dimensions of the hydrated Cs-SAPO-RHO are the same as the dehydrated one. Hydrated Cs-SAPO-RHO still possesses the space group of *I*23 instead of *I*432. It is distinct from the metal exchanged zeolite Rho whose structural distortion only occurred in the process of dehydration. Therefore, it can be clearly concluded that the distortion of the framework of SAPO-RHO is caused solely by the cations of Na^+ , K^+ , or Cs^+ .

The separation performance of the dehydrated H-SAPO-RHO and M-SAPO-RHOs ($\text{M} = \text{Na}, \text{K}, \text{and Cs}$) were first evaluated by the pure-component equilibrium adsorption isotherms for CO_2 , N_2 , and CH_4 at 273 K (Fig. S4), 298 K (Fig. 4a–c), and 313 K (Fig. S4) between 0–1 bar. The results in Fig. 4 and Fig. S4 show that all M-SAPO-RHOs have a higher uptake for CO_2 than for CH_4 and N_2 , and the uptake of all gases decreases with the increase of temperature. The CO_2 uptake at 298 K and 1 bar is in the order of H-SAPO-RHO (4.41 mmol g^{-1}) > Na-SAPO-RHO (3.53 mmol g^{-1}) > K-SAPO-RHO (0.87 mmol g^{-1}) > Cs-SAPO-RHO (0.45 mmol g^{-1}) (Fig. 4a, Table 1). A higher CO_2 (dynamic diameter of CO_2 : 0.33 nm) uptake in the H-SAPO-RHO at 1 bar is attributed

to the unblocked 8-ring pore openings and the small size of protons, leaving more room for CO_2 in *lta* cage, while it is of interest to note that an appreciable CO_2 uptake (1.21 mmol g^{-1} at 0.02 bar) is observed in the Na-SAPO-RHO although six Na^+ ions per unit cell occupy the elliptical *s8r* pore openings. It results from the fact that CO_2 with strong quadrupole moment can interact strongly with Na^+ ions and push them away instantaneously from the center of the *s8r*s to allow the CO_2 molecules to pass through, as observed as “trapdoor” effect.^[11, 14c, 15a, 19] In addition, an abrupt increase of CO_2 uptake on K-SAPO-RHO above 0.2 bar is observed. Such shape of the isotherm of CO_2 has been also observed in Na form of MER zeolite with 8MR window, which is attributed to the structure flexibility of the elliptical 8MR window in MER zeolite.^[20]

For CH_4 and N_2 , however, the adsorption on Na-SAPO-RHO is very limited ($0.027 \text{ mmol g}^{-1}$ at 0.98 bar for CH_4 and $0.070 \text{ mmol g}^{-1}$ at 0.85 bar for N_2), which might result from facts that 1) their dynamic diameters (CH_4 : 0.38 nm, N_2 : 0.36 nm) are larger than effective pore openings; 2) their weaker interactions with Na^+ ions are insufficient to push the Na^+ ions away from the center of the *s8r*s to allow the CH_4 and N_2 molecules to pass, i.e., the “trapdoor” remains shut. Notice that, gradual increase of the N_2 uptake on Na-SAPO-RHO with increase of pressure is observed as with H-SAPO-RHO (Fig. 4c) and the H form RHO zeolite.^[21] Elemental analysis shows that the exchange degree of Na^+ in Na-SAPO-RHO is ca. 87.13%, leaving 12.87% of H^+



balancing the negative charge of the framework of SAPO-RHO. Thus, the gradual increase of the N_2 uptake on Na-SAPO-RHO can be attributed to the existence of H^+ .

Different from the case in Na-SAPO-RHO, when the CO_2 , CH_4 , and N_2 pass through K-SAPO-RHO or Cs-SAPO-RHO, the K^+ or Cs^+ ions located in the center of $d8rs$ must first move from $d8r$ to $s8r$. Since K^+ or Cs^+ ions locate at the center of the $d8rs$ and coordinate with more framework oxygen atoms compared with Na^+ ions in the $s8r$, pushing K^+ or Cs^+ ions is energetically much more difficult than moving Na^+ ions. Thus, there is a lower uptake of CO_2 ($0.01 \text{ mmol} \cdot g^{-1}$ at 0.02 bar for both K-SAPO-RHO and Cs-SAPO-RHO), N_2 ($0.010 \text{ mmol} \cdot g^{-1}$ for K-SAPO-RHO and $0.014 \text{ mmol} \cdot g^{-1}$ for Cs-SAPO-RHO at 0.85 bar), and CH_4 ($0.024 \text{ mmol} \cdot g^{-1}$ for K-SAPO-RHO and $0.017 \text{ mmol} \cdot g^{-1}$ for Cs-SAPO-RHO at 0.98 bar) in the K-SAPO-RHO and Cs-SAPO-RHO than that in the Na-SAPO-RHO over the entire pressure range as expected (Table 1).

To further evaluate the selectivity of the M-SAPO-RHOs in the separation of CO_2/CH_4 and CO_2/N_2 , the separation factor α of CO_2/CH_4 (0.02/0.98 bar) and CO_2/N_2 (0.15/0.85 bar) were calculated on the basis of the single-component isotherms (Table 1). The separation factor is highly associated with the $CO_2/CH_4/N_2$ uptake at the operated pressure. As shown in Fig. 4b and 4c and Table 1, the CH_4 and N_2 uptakes at the pressure range for Na/K/Cs-SAPO-RHO is comparable and extremely low ($0.017 \sim 0.027 \text{ mmol} \cdot g^{-1}$ for CH_4 and $0.010 \sim 0.070 \text{ mmol} \cdot g^{-1}$ for N_2). The separation factor thus mainly depends on the uptake of CO_2 . Fig. 4d shows the CO_2 uptake of Na/K/Cs-SAPO-RHO at low pressure area and the separation factors for CO_2/CH_4 and CO_2/N_2 are summarized in Fig. 4e and 4f, respectively. The detailed uptakes for $CO_2/CH_4/N_2$ in SAPO-RHOs at various pressures and the corresponding values reported in the literature are provided in Table 1.

Significantly, the separation factor of 2196 of Na-SAPO-RHO for CO_2/CH_4 is twice more than that of 960, superior to all of the nanoporous materials reported to date (Table 1). The separation factor of Na-SAPO-RHO for CO_2/N_2 is also as high as 196, which is the top level among zeolitic materials. The unprecedented high separation factor of Na-SAPO-RHO for CO_2/CH_4 and CO_2/N_2 is in fact due to the much lower uptake of CH_4 ($0.027 \text{ mmol} \cdot g^{-1}$ at 0.98 bar) and N_2 ($0.070 \text{ mmol} \cdot g^{-1}$ at 0.85 bar) than that in all other nanoporous materials. We also evaluated the uptake rate (i.e., rate of adsorption) of M-SAPO-RHOs. Considering that the adsorption capacity for CH_4 and N_2 was very low, we measured only the rate of adsorption for CO_2 . The rate of adsorption curves for H-SAPO-RHO, Na-SAPO-RHO, K-SAPO-RHO, and Cs-SAPO-RHO at 298 K and 1.0 bar are provided in Fig. S5. As shown in Fig. S5, the rate of adsorption of H-SAPO-RHO and Na-SAPO-RHO is much higher than that of K-SAPO-RHO and Cs-SAPO-RHO, which is attributed the trapdoor effect caused by different cations.

To estimate the error in selectivity of the Na-SAPO-RHO, we prepared two more batches of the Na-SAPO-RHO (denoted as batches 2 and 3, the original Na-SAPO-RHO is denoted as batch 1) and conducted the N_2 adsorption/desorption (isotherms in Fig. S6 and textual properties in Table S5).

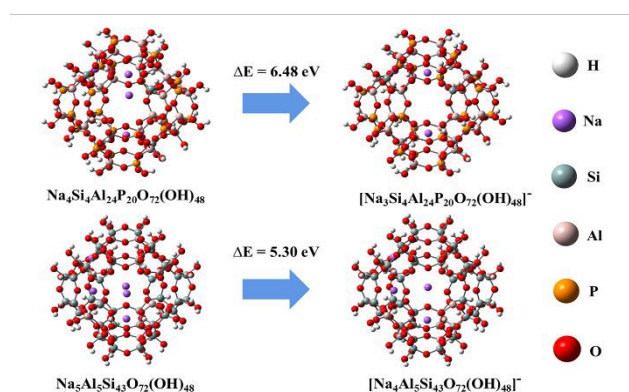


Fig. 5 Molecular structures of two neutral $Na_5Al_5Si_{43}O_{72}(OH)_{48}$ and $Na_4Si_4Al_{24}P_{20}O_{72}(OH)_{48}$ clusters and the binding energy of Na^+ in the center of elliptical $s8rs$ in two clusters.

Moreover, the pure component adsorption isotherms of CO_2 , CH_4 , and N_2 for the three batches of Na-SAPO-RHO were also measured (Fig. S7a-c) and the average uptake of CO_2 , CH_4 , and N_2 with error bars is plotted in Fig. S7d-f. As shown in Fig. S7, the adsorption capacity of the three batches of Na-SAPO-RHO for CO_2 , CH_4 , and N_2 is very similar to each other. The separation factors of the three batches of Na-SAPO-RHO for CO_2/CH_4 and CO_2/N_2 were calculated from their adsorption isotherms and plotted in Fig. S8a and b, respectively, which show that error in selectivity from batch to batch is very little.

To elucidate how the locations of inorganic cations affect the gas separation performance, we carried out the periodic DFT calculations using Vienna ab initio simulation package (VASP 5.4.4). The details of calculations are presented in Supporting Information. The results illustrate that N_2 and CH_4 have the weaker interactions with inorganic cations in the Na/K/Cs-SAPO-RHO framework than CO_2 does as shown in Table S6 and they only interact with inorganic cations locating in the $s6rs$. It is of significance to note that the CO_2 molecule in the Na-SAPO-RHO sample is captured by two Na^+ ions that are distributed in the $s6rs$ and $s8rs$, respectively (Fig. S9). However, it is distinct from the situations observed in K/Cs-SAPO-RHO in which CO_2 interacts with K^+/Cs^+ ions in the $s6rs$ solely (Fig. S11). These results indicate that the CO_2 molecule has a stronger interaction with Na-SAPO-RHO than with K/Cs-SAPO-RHO, which well explains a higher uptake of CO_2 in Na-SAPO-RHO than in K/Cs-SAPO-RHO at the low pressure.

To gain a deep understanding on the different performance between Na-SAPO-RHO and zeolite Na-Rho, density functional theory (DFT) calculations were conducted based on the cluster modes. As shown in Fig. 5, two neutral $Na_5Al_5Si_{43}O_{72}(OH)_{48}$ and $Na_4Si_4Al_{24}P_{20}O_{72}(OH)_{48}$ clusters cut from zeolite Na-Rho and Na-SAPO-RHO were utilized for the theoretical calculations. The details of calculations are presented in Supporting Information. The calculated results show that the energy required to push the Na^+ away from the center of the elliptical $s8rs$ of the



Na₅Al₅Si₄₃O₇₂(OH)₄₈ and Na₄Si₄Al₂₄P₂₀O₇₂(OH)₄₈ clusters is 5.30 eV and 6.48 eV, respectively. The results show that the Na⁺ ions have a stronger interaction with the SAPO framework than those with the aluminosilicate framework, indicating that the enhanced “trapdoor effect” in SAPO-RHO. This means that more energies would be needed for CO₂, CH₄, and N₂ to push the Na⁺ away from the center of the s8rs of Na-SAPO-RHO than from that of zeolite Na-Rho, leading to a lower uptake of CO₂/CH₄/N₂ in Na-SAPO-RHO than that in Na-Rho. The strong “trapdoor” effect is especially disadvantageous for CH₄ and N₂ to push Na⁺ away because the interaction between Na⁺ and CH₄ or N₂ is much weaker than that between Na⁺ and CO₂.^[11, 14c, 15a, 22] This explains the decrease of the uptake of CH₄ and N₂ in Na-SAPO-RHO is much more pronounced as compared to that of CO₂, resulting in a higher selectivity for CO₂.

The above results show that the Na-SAPO-RHO has a better performance than the K- and Cs-SAPO-RHO in the separation of CO₂/CH₄ and CO₂/N₂. Notice that the exchange degree in Na-SAPO-RHO is 87.13% upon 3 cycles of ion-exchange. To investigate the influence of ion-exchange degree on the separation performance, we further investigated the CO₂ separation of the Na-SAPO-RHOs with the exchange degree of 42.41, 72.64, and 100% upon 1, 2, and 4 cycles of ion-exchange process. The corresponding products are denoted as Na-1-SAPO-RHO, Na-2-SAPO-RHO, and Na-4-SAPO-RHO, respectively. The compositions and characterization results of these Na-

SAPO-RHOs are provided in Table S1, Fig. S12 and Fig. S13 in Supporting Information. DOI: 10.1039/D1SC00619C

The single component equilibrium adsorption isotherms of the Na-(1-4)-SAPO-RHOs at 298 K with the pressure up to 1 bar for CO₂, CH₄, and N₂ are displayed in Fig. S14 a, b, and c, respectively and the detailed uptakes of all components at various pressures are summarized in Table 1. The CO₂ uptakes of all Na-SAPO-RHOs at 0.02 and 0.15 bar are shown in Fig. S14 d. It is found that the uptake of CH₄ and N₂ gradually decreases with the increase of ion-exchange degree (CH₄: 0.090, 0.042, and 0.027 mmol g⁻¹ at 0.98 bar for 1, 2, and 3 cycles of exchanged samples, respectively; N₂: 0.116, 0.089, and 0.070 mmol g⁻¹ at 0.85 bar for 1, 2, and 3 cycles of exchanged samples, respectively) and reaches 0 at the 4 cycles of ion-exchange (Table 1 and Fig. S14b, c). Such results might be attributed to the strong “trapdoor” effect of Na⁺ on CH₄ and N₂ and the increased Na⁺ blocking of the s8r with the increase of exchanged Na⁺. Notice that, the Na-SAPO-RHO (3 cycles of ion-exchange) has the best CO₂ uptake capacity (1.21 mmol g⁻¹ at 0.02 bar) and selectivity performance ($\alpha(\text{CO}_2/\text{CH}_4)$: 2196; $\alpha(\text{CO}_2/\text{N}_2)$: 196) among the Na-SAPO-RHOs (Table 1 and Fig. S14e, f). This suggests that the amount and distribution of both Na⁺ and H⁺ in Na-SAPO-RHO play an important role in determining the gas adsorption. In this respect, further understanding is needed on the basis of future detailed structural characterizations and theoretical calculations.

Table 1. Comparisons of equilibrium CO₂ uptake and selectivity on various zeolites and SAPOs

Material	CO ₂ Uptake [mmol g ⁻¹]			CH ₄ Uptake [mmol g ⁻¹]	N ₂ Uptake [mmol g ⁻¹]	$\alpha(\text{CO}_2/\text{CH}_4)$ (0.02/0.98 bar)	$\alpha(\text{CO}_2/\text{N}_2)$ (0.15/0.85 bar)	Ref
	0.02 bar	0.15 bar	1.0 bar	0.98 bar	0.85 bar			
H-SAPO-RHO ^a	0.44	1.84	4.41	0.83	0.210	26	50	This work
Na-SAPO-RHO ^a	1.21	2.42	3.53	0.027	0.070	2196	196	This work
K-SAPO-RHO ^a	0.01	0.046	0.87	0.024	0.010	20	29	This work
Cs-SAPO-RHO ^a	0.01	0.054	0.45	0.017	0.014	30	22	This work
Na-1-SAPO-RHO ^a	0.81	2.04	3.43	0.090	0.116	441	105	This work
Na-2-SAPO-RHO ^a	0.71	2.28	3.38	0.042	0.089	828	145	This work
Na-4-SAPO-RHO ^a	0.60	1.82	3.08	0	0	∞	∞	This work
H-SAPO-RHO ^a	0.49	1.95	4.60	0.38	0.23	63	48	[24]
SAPO-34 ^b	0.24	1.20	3.26	0.65	---	20	---	[25]
Na-SAPO-34 ^b	0.89	2.10	3.40	0.62	0.26	75	44	[25]
SAPO-17 ^c	0.29	1.29	3.27	---	0.31	---	23	[26]
SAPO-35 ^c	0.29	1.87	3.68	---	0.32	---	33	[26]
SAPO-56 ^c	0.76	2.87	5.44	---	0.39	---	42	[26]
Na-RHO ^a	2.06	3.30	4.23	0.11	---	960	---	[15a]
Na-CHA ^a	2.64	3.95	4.70	1.60	0.60	81	37	[27]
Na-KFI ^d	---	3.40	---	---	0.27	---	71	[28]
Na-X ^a	2.00	3.17	5.00	0.67	0.23	147	78	[29]
Na-MER ^a	1.50	2.50	3.80	0.32	---	229	---	[30]
K-MER ^a	1.93	2.93	3.57	0.052	---	1818	---	[30]
NaKA (K=17%) ^a	1.00	2.30	3.43	---	0.02	---	660	[22]
Na-A ^a	3.20	3.90	4.80	1.34	0.65	117	34	[31]
Mg-MOF-74 ^a	2.30	5.65	8.00	1.11	---	102	---	[32]
SIFSIX-3-Zn ^a	1.95	2.30	2.55	0.79	0.46	121	28	[32a]
UTSA-280 ^a	0.48	1.58	2.78	0.10	0.15	235	60	[33]

Note: The adsorption data was measured at ^a298K, ^b293K; ^c273K, and ^d303K.



The breakthrough experiments of the Na-SAPO-RHO were conducted using binary CO₂/CH₄ (50/50, v/v) and CO₂/N₂ (15/85, v/v) gas mixtures at 298 K and atmospheric pressure (Schematic S1), mimicking the industrial process conditions of biogas^[2a, 23] and flue gas^[2a, 34] respectively and the corresponding breakthrough curves are given in Fig. S15. According to Fig. S15, CO₂ can be completely separated from CH₄ and N₂. On the basis of the breakthrough results, we also calculated the dynamic separation selectivity of the batch 1 of Na-SAPO-RHO for CO₂/CH₄ and CO₂/N₂ (Fig. S16 and Fig. S17). The detailed information for the calculation is included in the section 8 of the Supporting Information. As shown in Fig. S17, although the selectivity predicted by the breakthrough curves is slightly lower than that estimated from the multiple pure component adsorption measurements, Na-SAPO-RHO is also highly selective under dynamic conditions, rendering this zeolite potentially useful for selective CO₂ adsorption in practical application.

Conclusions

Silicoaluminophosphate **RHO** zeolite is hydrothermally synthesized in the presence of diethylamine as OSDA with the assistance of seed. Na⁺, K⁺, or Cs⁺ is introduced into the as-prepared SAPO-RHO via a direct ion-exchange and complete replacement of protonated diethylamine by Na⁺ while maintaining the zeolite crystallinity has been successfully achieved upon four cycles of ion-exchange. The structure of ion-exchanged SAPO-RHOs by three cycles is determined by Rietveld refinement. Structural analyses show that Na⁺ mainly site the center of *s8rs*, while the K⁺ and Cs⁺ ions are mainly distributed in the center of *d8rs*. Na⁺ ion-exchanged SAPO-RHO upon three cycles of ion-exchange (Na-SAPO-RHO) exhibits unprecedented separation factor of 2196 for CO₂/CH₄ and 196 for CO₂/N₂, which is much superior to K⁺ and Cs⁺ exchanged SAPO-RHOs with the same cycles of ion-exchange. Significantly, the Na⁺ form of SAPO-RHO exhibited an unprecedented separation for CO₂/CH₄, superior to all the nanoporous materials reported to date. Theoretical calculations show that the interaction between the Na⁺ and 8-rings in SAPO-RHO is much stronger than that in aluminosilicate Rho, which leads to a superior separation performance of Na-SAPO-RHO. Complete ion-exchange of Na⁺ in SAPO-RHO further increases the separation factor for CO₂/CH₄ and CO₂/N₂ by furtherly enhanced the “trapdoor” effect. Breakthrough experiments demonstrate that Na-SAPO-RHO can completely separate CO₂ from CH₄ or N₂. These superior features make Na-SAPO-RHO a promising candidate for CO₂ capture in natural gas purification and flue gas separation via adsorption-based separation processes. The present work introduces a new promising system based on silicoaluminophosphate zeolites for highly selective gas separation in terms of cation-tailored “trapdoor” effect.

Author Contributions

W.Y. and J.Y. designed and supervised the project; P.B. and Y.W. involved the design of the experiments; X.W., H.S., and B.W. performed the experiments; N.Y. and P.G. performed the structural analyses; M.X. and T.C. contributed to the calculations; P.L. and L.L. conducted the adsorption analyses; X.W. wrote the first draft; and W.Y., P.G. and J.Y. deeply revised the manuscript. X. W., N. Y., and M. X. contributed equally to this work.

Conflicts of interest

There are no conflicts to declare.

Acknowledgements

We acknowledge the financial support from the National Natural Science Foundation of China (U1967215, 21835002, 21621001) and the 111 Project of China (B17020). Dr. Peng Guo acknowledges financial support from the National Natural Science Foundation of China (No. 21972136), CAS Pioneer Hundred Talents Program (Y706071202), Dalian National Laboratory for Clean Energy, (DNL) Cooperation Fund, and Chinese Academy of Sciences (DNL201908). Dr. Nana Yan acknowledges financial support from the CAS Special Research Assistant Program and the scholarship from STOE.

Notes and references

- 1 M. E. Boot-Handford, J. C. Abanades, E. J. Anthony, M. J. Blunt, S. Brandani, N. Mac Dowell, J. R. Fernández, M.-C. Ferrari, R. Gross, J. P. Hallett, R. S. Haszeldine, P. Heptonstall, A. Lyngfelt, Z. Makuch, E. Mangano, R. T. J. Porter, M. Pourkashanian, G. T. Rochelle, N. Shah, J. G. Yao and P. S. Fennell, *Energy Environ. Sci.*, 2014, **7**, 130-189.
- 2 (a) Y.S. Bae and R. Q. Snurr, *Angew. Chem. Int. Ed.*, 2011, **50**, 11586-11596; (b) H. A. Patel, J. Byun and C. T. Yavuz, *ChemSusChem*, 2017, **10**, 1303-1317; (c) M. Pardakhti, T. Jafari, Z. Tobin, B. Dutta, E. Moharrer, N. S. Shemshaki, S. Suib and R. Srivastava, *ACS Appl. Mater. Interfaces*, 2019, **11**, 34533-34559.
- 3 (a) H. Yang, Z. Xu, M. Fan, R. Gupta, R. B. Slimane, A. E. Bland and I. Wright, *J. Environ. Sci.*, 2008, **20**, 14-27; (b) S. D. Kenarsari, D. Yang, G. Jiang, S. Zhang, J. Wang, A. G. Russell, Q. Wei and M. Fan, *RSC Adv.*, 2013, **3**, 22739-22773.
- 4 (a) R. T. Yang, *Gas Separation by Adsorption Processes*, Butterworth, Boston, 1987; (b) R. T. Yang, *Adsorbents: Fundamentals and Applications*, Wiley-Interscience, New York, 2003; (c) R. Ben-Mansour, M. A. Habib, O. E. Bamidele, M. Basha, N. A. A. Qasem, A. Peedikakkal, T. Laoui and M. Ali, *Applied Energy*, 2016, **161**, 225-255; (d) M. Khraisheh, S. Mukherjee, A. Kumar, F. Al Momani, G. Walker and M. J. Zaworotko, *J. Environ. Manage.*, 2020, **255**, 109874.
- 5 (a) A. H. Lu and G. P. Hao, *Annu. Rep. Prog. Chem., Sect. A: Inorg. Chem.*, 2013, **109**, 484-503; (b) J. Wang, L. Huang, R. Yang, Z. Zhang, J. Wu, Y. Gao, Q. Wang, D. O'Hare and Z.



- Zhong, *Energy Environ. Sci.*, 2014, **7**, 3478-3518; (c) S. Y. Lee and S. J. Park, *J. Ind. Eng. Chem.*, 2015, **23**, 1-11; (d) D. D. Zhou, X. W. Zhang, Z. W. Mo, Y. Z. Xu, X. Y. Tian, Y. Li, X. M. Chen and J. P. Zhang, *EnergyChem*, 2019, **1**, 100016.
- 6 (a) R. V. Siriwardane, M. S. Shen, E. P. Fisher and J. A. Poston, *Energy Fuels*, 2001, **15**, 279-284; (b) A. E. Creamer and B. Gao, *Environ. Sci. Technol.*, 2016, **50**, 7276-7289; (c) Z. Zhang, Z. P. Cano, D. Luo, H. Dou, A. Yu and Z. Chen, *J. Mater. Chem. A*, 2019, **7**, 20985-21003; (d) S. Wang, Y. Li, S. Dai and D.-E. Jiang, *Angew. Chem. Int. Ed.*, 2020, **59**, 19645-19648.
- 7 (a) K. T. Chue, J. N. Kim, Y. J. Yoo, S. H. Cho and R. T. Yang, *Ind. Eng. Chem. Res.*, 1995, **34**, 591-598; (b) J. Kim, L. C. Lin, J. A. Swisher, M. Haranczyk and B. Smit, *J. Am. Chem. Soc.*, 2012, **134**, 18940-18943; (c) O. Cheung and N. Hedin, *RSC Adv.*, 2014, **4**, 14480-14494; (d) Y.-Y. Wang, Q. Zhang and J.-H. Yu, *Chem. J. Chin. Univ.*, 2020, **41**, 616-622; (e) S.-S. Liu, Y.-C. Chai, N.-J. Guan and L.-D. Li, *Chem. J. Chin. Univ.*, 2021, **42**, 268-288.
- 8 (a) K. Sumida, D. L. Rogow, J. A. Mason, T. M. McDonald, E. D. Bloch, Z. R. Herm, T.-H. Bae and J. R. Long, *Chem. Rev.*, 2012, **112**, 724-781; (b) H. Furukawa, K. E. Cordova, M. O'Keeffe and O. M. Yaghi, *Science*, 2013, **341**, 1230444; (c) C. A. Trickett, A. Helal, B. A. Al-Maythaly, Z. H. Yamani, K. E. Cordova and O. M. Yaghi, *Nat. Rev. Mater.*, 2017, **2**, 17045; (d) Z. Hu, Y. Wang, B. B. Shah and D. Zhao, *Adv. Sustainable Syst.*, 2019, **3**; (e) Y. Jiang, P. Tan, S. Qi, C. Gu, S. Peng, F. Wu, X. Liu and L. Sun, *CCS Chem.*, 2020, **2**, 1659-1668; (f) V. Y. Mao, P. J. Milner, J.-H. Lee, A. C. Forse, E. J. Kim, R. L. Siegelman, C. M. McGuirk, L. B. Porter-Zasada, J. B. Neaton, J. A. Reimer and J. R. Long, *Angew. Chem. Int. Ed.*, 2020, **59**, 19468-19477.
- 9 (a) X. Hu, L. Liu, X. Luo, G. Xiao, E. Shiko, R. Zhang, X. Fan, Y. Zhou, Y. Liu, Z. Zeng and C. Li, *Appl. Energy*, 2020, **260**, 114244; (b) A. M. Varghese and G. N. Karanikolos, *Int. J. Greenhouse Gas Control*, 2020, **96**, 103005.
- 10 (a) J. Wu, F. Xu, S. Li, P. Ma, X. Zhang, Q. Liu, R. Fu and D. Wu, *Adv. Mater.*, 2019, **31**, 1802922; (b) F. Duan, X. Liu, D. Qu, B. Li and L. Wu, *CCS Chem.*, 2020, **2**, 2676-2687.
- 11 J. Shang, G. Li, R. Singh, Q. Gu, K. M. Nairn, T. J. Bastow, N. Medhekar, C. M. Doherty, A. J. Hill, J. Z. Liu and P. A. Webley, *J. Am. Chem. Soc.*, 2012, **134**, 19246-19253.
- 12 M. Palomino, A. Corma, J. L. Jordá, F. Rey and S. Valencia, *Chem. Commun.*, 2012, **48**, 215-217.
- 13 H. E. Robson, D. P. Shoemaker, R. A. Ogilvie and P. C. Manor, in *Molecular Sieves*, American Chemical Society, 1973, vol. 121, ch. 9, pp. 106-115.
- 14 (a) J. B. Parise and D. E. Cox, *J. Phys. Chem.*, 1984, **88**, 1635-1640; (b) J. B. Parise, T. E. Gier, D. R. Corbin, L. Abrams, J. D. Jorgensen and E. Prince, *J. Phys. Chem.*, 1984, **88**, 2303-2307; (c) M. M. Lozinska, J. P. S. Mowat, P. A. Wright, S. P. Thompson, G. L. Jorda, M. Palomino, S. Valencia and F. Rey, *Chem. Mater.*, 2014, **26**, 2052-2061; (d) S. R. G. Balestra, S. Hamad, A. R. Ruiz-Salvador, V. Domínguez-García, P. J. Merklings, D. Dubbeldam and S. Calero, *Chem. Mater.*, 2015, **27**, 5657-5667.
- 15 (a) M. M. Lozinska, E. Mangano, J. P. S. Mowat, A. M. Shepherd, R. F. Howe, S. P. Thompson, J. E. Parker, S. Brandani and P. A. Wright, *J. Am. Chem. Soc.*, 2012, **134**, 17628-17642; (b) M. M. Lozinska, E. Mangano, A. G. Greenaway, R. Fletcher, S. P. Thompson, C. A. Murray, S. Brandani and P. A. Wright, *J. Phys. Chem. C*, 2016, **120**, 19652-19662.
- 16 X. Su, P. Tian, J. Li, Y. Zhang, S. Meng, Y. He, D. Fan and Z. Liu, *Microporous and Mesoporous Mater.*, 2011, **144**, 113-119.
- 17 N. Yan, L. Wang, X. Liu, P. Wu, T. Sun, S. Xu, J. Han, P. Guo, P. Tian and Z. Liu, *J. Mater. Chem. A*, 2018, **6**, 24186-24193.
- 18 X. Xiang, M. Yang, B. Gao, Y. Qiao, P. Tian, S. Xu and Z. Liu, *RSC Adv.*, 2016, **6**, 12544-12552.
- 19 T. De Baerdemaeker and D. De Vos, *Nat. Chem.*, 2013, **5**, 89.
- 20 H. J. Choi, D. Jo, J. G. Min and S. B. Hong, *Angew. Chem. Int. Ed.*, 2021, **60**, 4307-4314. DOI: 10.1039/D1SC00619C
- 21 Q. Ke, T. Sun, X. Wei, Y. Guo, S. Xu and S. Wang, *Chem. Eng. J.*, 2019, **359**, 344-353.
- 22 Q. Liu, A. Mace, Z. Bacsik, J. Sun, A. Laaksonen and N. Hedin, *Chem. Commun.*, 2010, **46**, 4502-4504.
- 23 (a) K. Zhou, S. Chaemchuen and F. Verpoort, *Renewable and Sustainable Energy Rev.*, 2017, **79**, 1414-1441; (b) S. Wang, P. Bai, M. Sun, W. Liu, D. Li, W. Wu, W. Yan, J. Shang and J. Yu, *Adv. Sci.*, 2019, **6**, 1901317.
- 24 X. Su, P. Tian, D. Fan, Q. Xia, Y. Yang, S. Xu, L. Zhang, Y. Zhang, D. Wang and Z. Liu, *ChemSusChem*, 2013, **6**, 911-918.
- 25 Y. Luo, H. H. Funke, J. L. Falconer and R. D. Noble, *Ind. Eng. Chem. Res.*, 2016, **55**, 9749-9757.
- 26 O. Cheung, Q. Liu, Z. Bacsik and N. Hedin, *Microporous and Mesoporous Mater.*, 2012, **156**, 90-96.
- 27 Y. Guo, T. Sun, Y. Gu, X. Liu, Q. Ke, X. Wei and S. Wang, *Chem. Asian J.*, 2018, **13**, 3222-3230.
- 28 Q. Liu, T. Pham, M. D. Porosoff and R. F. Lobo, *ChemSusChem*, 2012, **5**, 2237-2242.
- 29 K. S. Walton, M. B. Abney and M. Douglas LeVan, *Microporous and Mesoporous Mater.*, 2006, **91**, 78-84.
- 30 V. M. Georgieva, E. L. Bruce, M. C. Verbraeken, A. R. Scott, W. J. Casteel, S. Brandani and P. A. Wright, *J. Am. Chem. Soc.*, 2019, **141**, 12744-12759.
- 31 P. Rzepka, D. Wardecki, S. Smeets, M. Müller, H. Gies, X. Zou and N. Hedin, *J. Phys. Chem. C*, 2018, **122**, 17211-17220.
- 32 (a) P. Nugent, Y. Belmabkhout, S. D. Burd, A. J. Cairns, R. Luebke, K. Forrest, T. Pham, S. Ma, B. Space, L. Wojtas, M. Eddaoudi and M. J. Zaworotko, *Nature*, 2013, **495**, 80-84; (b) Z. R. Herm, J. A. Swisher, B. Smit, R. Krishna and J. R. Long, *J. Am. Chem. Soc.*, 2011, **133**, 5664-5667.
- 33 R. Lin, L. Li, A. Alsalmeh and B. Chen, *Small Structures*, 2020, **1**, 2000022.
- 34 J. K. Bower, D. Barpaga, S. Proding, R. Krishna, H. T. Schaef, B. P. McGrail, M. A. Derewinski and R. K. Motkuri, *ACS Appl. Mater. Interfaces*, 2018, **10**, 14287-14291.

